Multiuser Entanglement Distribution in Quantum Networks Using Multipath Routing

EVAN SUTCLIFFE[ID] **(Member, IEEE),**
AND ALEJANDRA BEGHELLI[ID] **(Member, IEEE)**
Optical Networks Group, Electronic & Electrical Engineering Department, University College London, WC1E 7JE London, U.K.

Corresponding author: Evan Sutcliffe (e-mail: evan.sutcliffe.20@ucl.ac.uk).

ABSTRACT Quantum networks facilitate numerous applications including secure communication and distributed quantum computation by performing entanglement distribution. For some multiuser quantum applications, access to a shared multipartite state is required. We consider the problem of designing protocols for distributing such states, at an increased rate. For this, we propose three protocols that leverage multipath routing to increase the distribution rate for multiuser applications. The protocols are evaluated on quantum networks with noisy intermediate scale quantum (NISQ) constraints, including limited quantum memories and probabilistic entanglement generation. Simulation results show that the developed protocols achieve an exponential increase in the distribution rate of multipartite states compared to single-path routing techniques, with a maximum increase of four orders of magnitude for the cases studied. Furthermore, the relative increase in the distribution rate was also found to improve for larger sets of users. When the protocols were tested in scaled-down real-world topologies, it was found that a topology had a significant effect on the multipartite state distribution rates achieved by the protocols. Finally, we found that the benefits of multipath routing are maximum for short quantum memory decoherence times and intermediate values of entanglement generation probability. Hence, the protocols developed can benefit NISQ quantum network control and design.

INDEX TERMS Distributed quantum computation, Greenberger–Horne–Zeilinger (GHZ) states, multipartite, quantum communication, quantum internet.

I. INTRODUCTION

A quantum network is a collection of devices that can exchange quantum information over quantum channels [1]. This can be achieved by first distributing a shared entangled state between the users that wish to exchange quantum information and then performing quantum teleportation [2], [3]. Communicating between two users requires a 2-qubit (bipartite) entangled state. For multiple users to have access to a shared entanglement, a multiqubit (multipartite) state must be distributed. Applications that can use shared multipartite states include clock synchronization [4], distributed quantum sensing [5], secret sharing [6], [7], and multiparty quantum key distribution (QKD) [8]. A further key motivation for quantum communication is quantum computation, due to the benefits of running quantum algorithms distributed over multiple quantum computers [9], [10], [11]. In such

cases, multipartite states can be used to facilitate multiqubit operations or for quantum error correction between multiple devices [12], [13].

Sharing multipartite states between distant users requires the design of multiuser entanglement distribution protocols. Many protocols assume the generation of bipartite entanglement between a central device and each user, which are then transformed into a multipartite state by performing local operations in the central device [14], [15], [16]. If the user is not directly connected to the center node by a network edge, a long-distance entanglement can be distributed by entanglement swapping, along a precomputed route of quantum repeaters [17], [18]. A key drawback to such approaches is that in quantum networks, precomputed single-path (SP) routing has a low rate of success, which decreases with the distance between users. This issue is compounded when sharing

entanglement between multiple users. A secondary drawback is that the number of quantum memories at the central device can constrain the number of users an entangled state can be distributed between.

We propose three multiuser entanglement distribution protocols that can overcome some of the limitations of using single precomputed paths. The proposed protocols perform routing by dynamically selecting a path, using knowledge of the successfully distributed entanglement states. In designing such protocols, we consider current quantum computers, described as noisy intermediate scale quantum (NISQ) devices due to their limited number of qubits and noisy operations. Therefore, we consider multipartite state distribution protocols for networks constrained by their available quantum resources. Due to their uses in quantum computation and secret-sharing applications [19], [20], the protocols developed focus on the distribution of the maximally entangled Greenberger–Horne–Zeilinger (GHZ) states.

The rest of this article is organized as follows. Section II discusses the previous work and highlights the contribution of this article. Section III describes the network model and assumptions while Section IV gives the problem statement for this article. The protocols are presented in Section V and the performance evaluation results are reported in Sections VI and VII. Analytical upper bounds and approximations for the distribution rate (DR) are derived in Section VIII. Finally, Section IX concludes this article.

II. PREVIOUS WORK AND CONTRIBUTION

We classify previous work using two main features: 1) the size of the entangled state to be distributed (bipartite versus multipartite) and 2) the routing strategy used [SP versus multipath (MP)]. For SP routing, Bell pair generation is attempted over the network edges of a unique precomputed path (or tree for the multipartite case). In contrast, MP routing attempts Bell pair generation over all network edges and selects the best possible path or tree using only those edges where Bell pairs are present. For SP and MP, we use the term "path" loosely, as a tree is not a path.

A. SP ROUTING FOR BIPARTITE STATES

In a quantum network, an SP routing protocol works by selecting an SP of quantum channels, which connects two users, such that the end-to-end DR is maximized [18], [21], [22]. This approach parallels that of shortest-path (SP) routing in classical networks. For a network of noisy quantum channels, approaches can be taken to improve the DR and fidelity of the distributed states [22], [23].

B. SP ROUTING FOR MULTIPARTITE STATES

For multipartite state distribution, the routing is necessarily more complex. Multipartite states of N qubits can be distributed to a set of S users, where $|S| \leq N$. We focus on the case $N = |S|$ with each party receiving a single qubit of the multipartite state. Some multipartite SP routing protocols extended the concept of bipartite SP routing by precalculating paths between the users and a central device [14], [15], [16], [24] and then generating a Bell pair between the central device and each of the users. A multipartite state can then be generated from these Bell pairs using only local (qubit) operations and classical communication (LOCC). The route selection can also be performed with secondary parameters, such as fidelity or time delay [14]. By allowing SP routing along a tree of edges connecting the users, a central device is no longer required. However, this approach has an additional classical communication cost [14], [22], [25].

C. MP ROUTING FOR BIPARTITE STATES

Using MP routing, a practical entanglement distribution protocol was developed by Pant et al. [26], building on results by Pirandola [27] and Acín et al. [28]. In the grid topologies studied, the MP protocol achieved a higher end-to-end DR than those that employ SP routing strategies. In addition, the end-to-end DR did not degrade with distance among users, as long as the Bell pairs between adjacent nodes were generated above a given threshold probability. This is a significant improvement on the exponentially decaying rate–distance relationship achieved by SP routing [29].

This distance-independent behavior of MP routing can be explained in terms of the bond percolation problem. For certain graphs where edges are created probabilistically, a giant connected component (GCC) of $O(|V|)$ nodes emerges when edges are generated above a critical threshold probability p_c [30], [31], [32], where $|V|$ is the number of network nodes. For grid lattice topologies, $p_c = 0.5$, and hence, percolation is observed for $p > 0.5$. In quantum networks, Bell pairs between adjacent nodes can represent the probabilistically generated edges of the bond percolation problem. Therefore, two nodes being in the same connected component means a path of edges exists where every edge holds an entanglement link. By performing Bell state measurements (BSMs) at all nodes along such a path, a long-distance Bell pair can be distributed between these users. When Bell pairs between adjacent nodes are generated above p_c, the likelihood of a path existing is independent of the distance between the nodes, and hence, the rate of entanglement distribution is independent of distance.

The work of Pant et al. [26] has since been extended by other authors, such as improved protocols for networks of imperfect repeaters, multitimestep network models, or for sharing 3-qubit GHZ states between two users [33], [34], [35], [36]. Some MP protocols require global knowledge of the distribution of the entangled states over the network [26]. Other protocols are developed to utilize local knowledge only [35]. This latter approach can reduce the classical communication requirements. However, this approach generates large intermediate entangled states, which can reduce the fidelity of the distributed state.
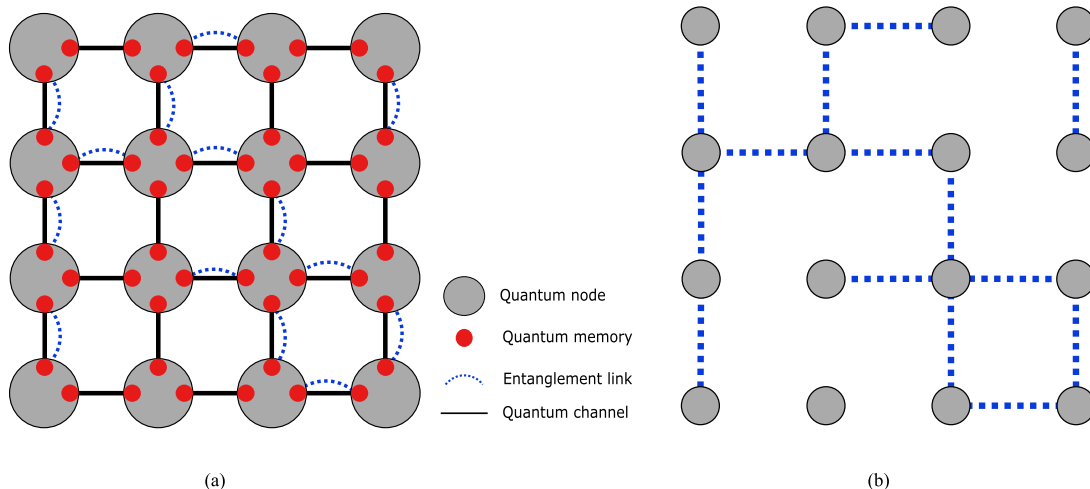
FIGURE 1. (a) Diagram of a quantum network defined by a graph *G* in a 4 × 4 grid topology. Also shown is a random set of entanglement links shared between adjacent nodes. (b) Subgraph $G' = (V, E')$ with edges from *G* with $\omega(e) = 1$.

D. MP ROUTING FOR MULTIPARTITE STATES

MP routing has not been applied to distributing multipartite states between multiple users, except for preliminary results in [37] and [38]. In [38], two MP protocols, MP-G and MP-C, for multipartite entanglement distribution are proposed and evaluated in grid topologies. MP-G extends previous work using a central node by allowing multiple paths to be considered between the central node and each user. The paths are selected considering all edges for which Bell pairs between adjacent nodes are present. MP-C (also discussed in this article) discards the use of a central node by performing routing using the Steiner tree, which connects all the users. Both MP protocols achieved significantly higher multipartite DRs than SP approaches. The work in [38] was extended in [37] to evaluate the performance of MP-G and MP-C in real-world topologies, where the better performance of MP routing was again confirmed.

E. EXTENSION TO PREVIOUS WORK

This article extends our previous work by the following:

1) proposing the new protocols MP-P and MP-G+;
2) describing the proposed protocols in detail by means of pseudocode and providing expressions for their routing computational complexity and classical communication complexity;
3) evaluating the performance of the protocols under new scenarios;
4) extending the results in [37] by evaluating the performance of the new MP-P protocol in mesh topologies;
5) providing an analytical approximation of the DR for the best performing MP protocols.

Overall, the contribution of this article consists of presenting consolidated results that address, for the first time, the problem of multiuser entanglement distribution using MP routing.

III. NETWORK MODEL AND ASSUMPTIONS

A. QUANTUM NETWORK MODEL

A quantum network can be represented as a graph $G = (V, E)$, with a set of nodes *V* and edges *E*. An example 4 × 4 grid topology is shown in Fig. 1(a).

Edges represent quantum channels, over which *entanglement links* can be generated. An entanglement link is a maximally entangled 2-qubit state, shared between adjacent nodes in a quantum network. We assume entanglement links are distributed in the form of a $|\phi^+\rangle = \frac{1}{\sqrt{2}}(|00\rangle + |11\rangle)$ state. For clarity, we, henceforth, refer to the $|\phi^+\rangle$ state as an *entanglement link* when shared between adjacent nodes (as in Fig. 1), and as a *Bell pair* when shared between distant users by entanglement swapping.

Distributing entanglement links over a noisy quantum channel is lossy and, hence, probabilistic. The probability p_e of successfully generating an entanglement link over an edge $e \in E$ can be modeled as

$$p_e = p_{op}(1 - p_{loss}) \qquad (1)$$

where p_{op} denotes the probability of imperfect node operations in entanglement link generation and p_{loss} the probability of qubit loss in the channel [18]. If we assume photonic qubits with channels of optical fiber, then for a channel of length *L* km with attenuation 0.2 dB/km, this loss can be expressed as $p_{loss} = 1 - 10^{-0.2L/10}$. The operation probability p_{op} represents a lumped probability of generating an entanglement link for two back-to-back devices (e.g., at $L = 0$ km), thus excluding photon loss in the fiber from p_{op}. Factors that can affect p_{op} include failure in photon generation, imperfect qubit-photon entanglement, or photon frequency conversion [18], [39].

Nodes represent devices able to store qubits in quantum memories and perform LOCC. We assume all nodes have equal capabilities and can perform any function (e.g., as a
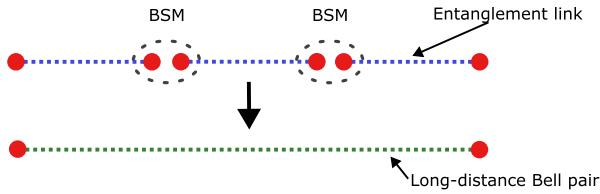
FIGURE 2. Entanglement swapping is performed to distribute a long-distance Bell pair from a path of entanglement links. This is achieved by performing BSMs on the qubits at intermediate nodes. Entanglement links and Bell pairs are both $|\phi^+\rangle$ states.

user, repeater, or center node). Thus, any nodes in the network can request to share a multipartite state. The capabilities are as follows.

1) All nodes have a single quantum memory per edge, allocated for communication purposes.
2) When an entanglement link is successfully generated over a network edge, entangled qubits are stored in specified quantum memories at the adjacent nodes connected to that edge. While the quantum memories are occupied by an entanglement link, they cannot be reused for a new entanglement link generation process.
3) All quantum memories have identical decoherence times. The quantum memories are modeled using a cut-off decoherence of time T_c. That means that before T_c, a qubit is stored in the quantum memory with perfect fidelity. After T_c, the qubit is assumed to have undergone decoherence and is discarded [21].
4) All LOCC operations are error-free, e.g., all nodes can perform error-free local operations between qubits stored in any quantum memory. Error-free classical communication is enabled by a parallel classical network.

The main LOCC operations used for distributing multipartite states are entanglement swapping and entanglement fusion. Entanglement swapping allows for the distribution of long-distance entanglement along a path of quantum repeaters. As we assume the devices can freely select any two qubits when performing entanglement swapping, these nodes could also be defined as quantum switches[1] [41], [42]. A Bell pair can be shared between distant nodes by entanglement swapping [17], [18]. By performing a BSM on the qubits of entanglement links at each intermediate node along the path, a long-distance Bell pair is distributed, such as shown in Fig. 2.

A N-qubit GHZ state can be generated by entanglement fusion using at least $N-1$ Bell pairs. The N-qubit GHZ state is given as $|\mathrm{GHZ}_N\rangle = \frac{1}{\sqrt{2}}(|0\rangle^{\otimes N} + |1\rangle^{\otimes N})$. The $|\phi^+\rangle$ state is equivalent to a $|\mathrm{GHZ}_2\rangle$ state. The entanglement fusion operation combines two GHZ states of qubit sizes n_1 and n_2 and entangles them, to generate a single state of size $n_1 + n_2 - 1$.

---

[1]This definition of a quantum switch should not be confused with a different definition, in which a quantum switch refers to using a qubit to control the operation order of a circuit [40].

This operation is executed at a node by entangling a qubit from each state, by measuring one of the qubits and then performing corrections depending on the measurement outcome. These deterministic operations can be performed iteratively to generate large multipartite states [25], [43]. Similarly, a BSM can combine two GHZ states into a single state of size $n_1 + n_2 - 2$ [24]. Fig. 3 shows the generation of a 4-qubit GHZ state from four Bell pairs. By generating GHZ states from multiple Bell pairs, multipartite states can be shared across a quantum network without requiring all qubits to be successfully transmitted along a separate point-to-point connection for each user.

B. QUANTUM NETWORK OPERATION ASSUMPTIONS

Link-state information: The binary variable $\omega(e) \in \{0, 1\}$ is a state that represents if an entanglement link is present $\omega(e) = 1$, or absent $\omega(e) = 0$ over an edge e. The subgraph $G' = (V, E')$, as shown in Fig. 1(b), can represent the global link-state, of $\omega(e)$ for all $e \in E$ over a network. The edges E' are the subset of E for which $\omega(e) = 1$. We assume that global link-state information G' is available for network operations. The knowledge of the link state is made possible by heralded entanglement distribution, where success is flagged by a classical signal [44]. Collating the global link-state information will have an associated classical communication and time delay cost. Evaluating such costs is out of the scope of this work.

Time-slotted operation: We assume a discrete-time network operation model. Each timeslot lasts for time T_{slot}, and thus, an entanglement link can be stored (i.e., $\omega(e) = 1$) over an overedge for up to Q_c timeslots ($Q_c = \lfloor T_c/T_{\mathrm{slot}} \rfloor$) from generation [23]. After an entanglement link has been stored for over Q_c timeslots, it is discarded ($\omega(e) = 0$). This means that $\omega(e)$ varies over multiple timeslots. This temporal variation is described by the sequence $\Omega_T = (\omega(e)_1, \omega(e)_2, \ldots \omega(e)_T)$, where $\omega(e)_t$ is the state of $\omega(e)$ in timeslot t and T is the network operation period, measured in number of timeslots. If a N-qubit GHZ state is not successfully established in one timeslot, the protocol reattempts distribution in future timeslots. In these future timeslots, only entanglement links that are still present (i.e., within Q_c timeslots since generation) plus newly generated entanglement links can be used to find a routing solution R.

IV. PROBLEM STATEMENT

Consider a quantum network represented by the graph $G = (V, E)$ with a subset of vertices $S \in V$, requesting an N-qubit GHZ state to be shared among them. In this article, the problem of *multipartite entanglement distribution* consists of generating a $|\mathrm{GHZ}_N\rangle$ state between users S with $|S| > 2$ and $N = |S|$, such that the rate at which the GHZ state is generated per time slot is maximized. We call this the *distribution rate* and denote it by DR.

To generate a $|\mathrm{GHZ}_N\rangle$ state, a routing solution R must be found. The routing solution represents a set of entanglement
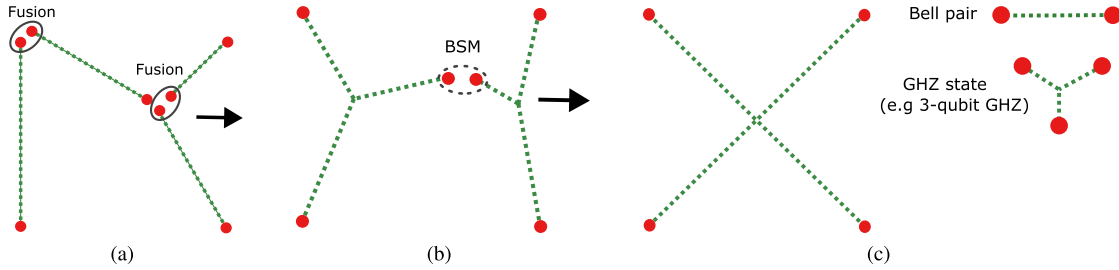
FIGURE 3. Example of the distribution of a $|GHZ_4\rangle$ state from four Bell pairs. GHZ states are shown using a star symbology, which is not equivalent to the graphical notation of a graph state. (a) Two entanglement fusion operations are performed, combining four Bell pairs into two $|GHZ_3\rangle$ states. (b) Two $|GHZ_3\rangle$ states are then combined by a BSM to generate a c) $|GHZ_4\rangle$ state between the desired qubits.

links, which can be combined by LOCC operations to generate the required GHZ state. A *multipartite entanglement distribution protocol* specifies the set of rules for finding a solution to the problem described earlier.

We assess the performance of the protocols developed in terms of the DR, defined as the average number of GHZ states distributed per timeslot $DR = \frac{\#GHZ}{T_{slot}}$. This metric does not take into account the size of the GHZ state distributed. Furthermore, the DR should not be confused with the rate at which entanglement links are distributed between adjacent nodes.

V. MULTIPARTITE DISTRIBUTION PROTOCOLS
A. BENCHMARK SOLUTION (SP PROTOCOL)

For comparison purposes, a generalized version of a multipartite SP protocol is used as a benchmark, denoted as the SP protocol. The SP protocol utilizes a central node and only attempts entanglement link generation along pre-calculated SPs from a central node to each user [14], [24]. These paths together describe the routing solution R.

The operations performed by the SP protocol are described in Algorithm 1. Initially, the center node v_c is selected (line 2) using an exhaustive strategy: for each candidate center node $v \in V$, with a nodal degree ($\deg(v)$) greater than or equal to $|S|$, a routing solution R_v is found using a max-flow routing algorithm [45]. Next, the center node v_c is selected such that $DR_{SP}(v_c) \geq DR_{SP}(v) \ \forall \ v \in V$ with $\deg(v) \geq |S|$. For the SP protocol, the value of $DR_{SP}(v)$ can be found directly from the routing solution

$$DR_{SP}(v) = \prod_{e \in R_v} p_e. \quad (2)$$

If no valid routing solution R_v can be found for the candidate node v then $DR_{SP}(v) = 0$. A valid routing consists of an edge-disjoint path between each user and the center node. The paths must be edge-disjoint due to the assumption that nodes can only store a single entanglement link per edge and because entanglement links are consumed by entanglement swapping. As there must be $|S|$ edge-disjoint paths between v_c and each user in S, the center node must have a nodal degree greater than or equal to $|S|$.

The selection of the center node v_c is performed before multipartite state generation is attempted and remains fixed

Algorithm 1: SP Protocol.

1: **function** SP(G, S)
2:   v_c = selectCentreNode(G, S)
3:   R = getShortestPaths(G, v_c, S)
4:   hasGHZ = **False**
5:   **while** *not* HasGHZ **do**
6:     SimulateEntanglementLinks(G)
7:     G' = updateLinkSubgraph(G)
8:     S' = $S-\{$ hasSharedBellPair(G, v_c, S) $\}$
9:     **for** $s \in S'$ **do**
10:       **if** $R[s] \in G'$ **then**
11:         entanglementSwapping($G, R[s], v_c, s$)
12:         G' = updateLinkSubgraph(G)
13:       **end if**
14:     **end for**
15:     **if** hasSharedBellPair(G, v_c, S) == S **then**
16:       entanglementFusion(G, v_c, S)
17:       hasGHZ = **True**
18:     **end if**
19:   **end while**
20: **end function**

throughout the operation of the protocol. In grid topologies with uniform p_e, the center node selection is reduced to selecting the centroid of the users. The routing solution computed for the selected central node is stored as R (line 3).

Next, the protocol runs for multiple timeslots, terminating once a GHZ state is generated (lines 5–19). At the start of each timeslot, the entanglement link generation is attempted over all edges in R, and qubit decoherence of the network model is simulated (line 6), meaning any entanglement links older than Q_c timeslots are discarded. The state of G' is then updated (line 7). The protocol operates to generate a Bell pair shared between the center node and each user. To do so, the protocol first obtains the subset of users S', which do not currently hold a Bell pair shared with the center node (line 8). For each of these users $s \in S'$, the precomputed path $R[s]$ between s and the center node is checked to assess if all edges in the path $R[s]$ hold an entanglement link (line 10). If so, a Bell pair is generated by performing entanglement swapping along the path (line 11), and G' is updated (line 12). When

all users share a Bell pair with the center node (line 15), the GHZ state is generated by performing entanglement fusion between the qubits of the Bell pairs held in the center node (line 16).

B. PROPOSED MP PROTOCOLS

We propose three protocols, which are novel variants of MP routing applied to distributing a multipartite state between multiple users. The proposed MP protocols are the Greedy Plus (MP-G+), Cooperative (MP-C), and Packing (MP-P) protocols.

In each timeslot, the MP protocols perform the following three distinct operations.

1) *Entanglement link generation:* Nodes attempt to generate entanglement links over all the edges in G.
2) *MP routing:* The protocols attempt to compute a *routing solution* using the global link-state information represented as the subgraph G'. Unlike SP, where the routing solution is made of edges in G, the routing solution of MP protocols only consists of edges in G', which are known to hold entanglement links.
3) *GHZ state generation:* If a routing solution was found, an N-qubit GHZ state is generated from the selected entanglement links. This is done such that the qubits of the GHZ state are shared among the users S.

1) MP GREEDY (MP-G+)

The MP-G+ protocol extends the ideas of the SP protocol described in Section V-A by allowing MP routing. Similarly to the SP protocol, a valid routing solution consists of an edge-disjoint path between the center node and each user. However, whereas the SP protocol uses a single precomputed set of paths in which entanglement link generation is reattempted each timeslot, the MP-G+ protocol can select paths from any edges in G'. By routing paths over G', the routing solution only uses edges that hold entanglement links. For the MP protocols, a routing solution is valid if a route can be found from edges that hold entanglement links. Each path of entanglement links can be used to generate a Bell pair. Once a Bell pair has been shared with each user, a GHZ state is then generated by performing entanglement fusion at the center node.

The MP-G+ protocol is described in Algorithm 2. First, a center node is selected using the same subprocedure as for the SP protocol (line 2). This selection maximizes the DR for the SP protocol; therefore, is considered a suitable center node for the MP-G+ protocol.

Next, the MP-G+ protocol executes over multiple timeslots to generate a GHZ state (lines 4–17). At the start of a timeslot, the entanglement link generation and qubit decoherence are simulated (line 5) and the state of G' (line 6) is updated. Then, the protocol identifies the subset S', made of users that do not currently share a Bell pair with the center node (line 7). A routing solution of valid paths is then found between the center node and as many users in S'

Algorithm 2: MP-G+ Protocol.

1: **function** MP-G+(G, S)
2: $\quad v_c = $ selectCentreNode(G, S)
3: $\quad$ hasGHZ $= $ **False**
4: $\quad$ **while** *not* HasGHZ **do**
5: $\quad\quad$ simulateEntanglementLinks(G)
6: $\quad\quad G' = $ updateLinkSubgraph(G)
7: $\quad\quad S' = S - \{$ hasSharedBellPair$(G, v_c, S) \}$
8: $\quad\quad R = $ getShortestPaths(G', v_c, S')
9: $\quad\quad$ **for** *path* $\in R$ **do**
10: $\quad\quad\quad$ entanglementSwapping$(G, path, v_c, s)$
11: $\quad\quad\quad G' = $ updateLinkSubgraph(G)
12: $\quad\quad$ **end for**
13: $\quad\quad$ **if** hasSharedBellPair$(G, v_c, S) == S$ **then**
14: $\quad\quad\quad$ entanglementFusion(G, v_c, S)
15: $\quad\quad\quad$ hasGHZ $= $ **True**
16: $\quad\quad$ **end if**
17: $\quad$ **end while**
18: **end function**

---

as possible while using the fewest number of entanglement links (line 8). To do so, the set of edge-disjoint paths between a single-source (center node) and multisinks (users in S'), where each sink can only utilize an SP, are computed for each timeslot using a max-flow approach algorithm [45], [46]. Routing using this approach is an improvement to the initial MP Greedy (MP-G) protocol proposed in [38], where a path between the center node and each user was found iteratively as the SP in G'. Notice that a valid path might not be found for every user in S' in the same timeslot. In practice, the MP-G+ was found to achieve only a small improvement in the DR compared to the original MP-G protocol [38].

For each path stored in R, a Bell pair is shared between the center node and the specific user by entanglement swapping (line 10) and the link-state information in G' is updated (line 11). If all users in S share a Bell pair with the central node, then a GHZ state is finally generated (lines 13–14).

An example routing solution of the MP-G+ protocol is shown in Fig. 4, where it can be seen that the SPs in G' are not necessarily the SPs in the underlying network topology G.

2) MP COOPERATIVE (MP-C)

The MP-C protocol is a multipartite entanglement distribution protocol, which relaxes the constraint of requiring a central node. Instead, a GHZ state can be generated from a tree of entanglement links, which connects the users in S. By using a Steiner tree as the routing solution R a GHZ state can be distributed using the fewest number of entanglement links possible. Fig. 4 illustrates the operation of the MP-C protocol where users are connected by a Steiner tree of entanglement links.
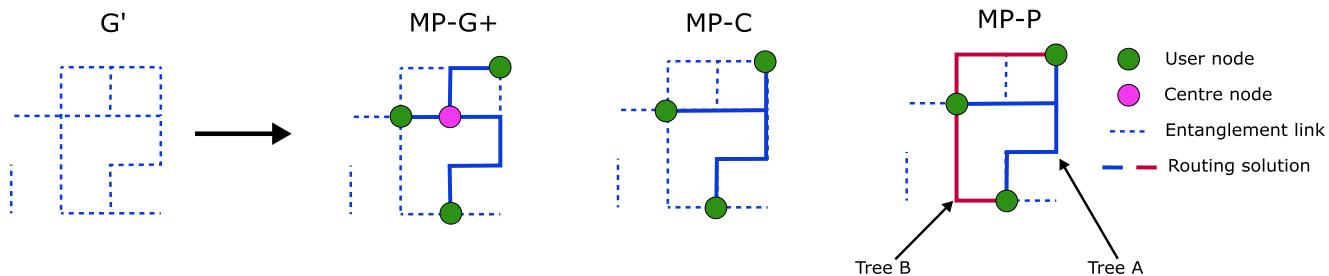
FIGURE 4. Routing solutions for the MP-G+, MP-C, and MP-P protocols for three users in an example state of G'. The MP-G+ protocol finds the minimum distance edge-disjoint paths in G' to connect the users to a preselected center node. For this example, this requires seven entanglement links. The MP-C and MP-P both use a routing solution consisting of the Steiner tree (using 6 links). However, for the MP-P protocol, multiple GHZ states can be generated if multiple Steiner trees can be found in G'. The example shows a situation where two $|GHZ_3\rangle$ states can be generated (Trees A and B).

The MP-C protocol is described in Algorithm 3. The protocol runs for multiple timeslots until a GHZ state is distributed (lines 3–12). At the start of each timeslot, entanglement link generation, and the qubit decoherence are simulated (line 4) and G' is updated (line 5). The protocol then checks if all users are in the same connected component in G' (line 6). This is a sufficient condition for the existence of a connecting tree of entanglement links between them. Therefore, the routing solution is found as the Steiner tree in G' that connects S (line 7). A GHZ state is generated from the entanglement links along the routing solution by entanglement swapping and entanglement fusion operations (lines 8–9). First, by performing entanglement swapping, the entanglement links along R are converted into long-distance Bell pairs, which are shared between the users and nodes in the Steiner tree that have a nodal degree greater than two. The GHZ state is generated by performing entanglement fusion operations at all nodes in the Steiner tree, which hold multiple qubits (line 9).

By routing using a Steiner tree, the MP-C protocol does not require a central node and the routing solution will on average require fewer entanglement links. However, this means that entanglement fusion operations might be required at multiple nodes when generating a GHZ state. The LOCC operations required are, therefore, more complex compared to the MP-G+ and SP protocols, where entanglement fusion is performed only at the center node. In addition, a potential drawback to MP-C is that without a fixed center node, the protocol must wait until all users can be connected by a Steiner tree in the same timeslot. This contrasts with the MP-G+ and SP protocols, in which the generation of a Bell pair between each v_c-user pair can be performed as soon as a path exists, with the GHZ state being generated once all users share a Bell pair with the center node.

3) MP PACKING (MP-P)

The MP-G+ and MP-C protocols attempt to distribute a single GHZ state per timeslot. If there are multiple edge-disjoint trees in G', multiple GHZ states can be generated between the same set of users. Fig. 4 shows an example where the MP-P protocol can generate two GHZ states for a single instance

---

Algorithm 3: MP-C Protocol.

```
 1: function MP-C(G, S)
 2:    HasGHZ = False
 3:    while not HasGHZ do
 4:        SimulateEntanglementLinks(G)
 5:        G' = updateLinkSubgraph(G)
 6:        if hasConnectingTree(G', S) then
 7:            R = minimumSteinerTree(G', S)
 8:            EntanglementSwapping(G, R, S)
 9:            EntanglementFusion(G, R, S)
10:            HasGHZ = True
11:        end if
12:    end while
13: end function
```

of G'. This can improve the multipartite DR or benefit applications that require multiple copies of a multipartite state. These include QKD [47], or entanglement distillation, when multiple copies of a state can be combined to improve the average fidelity of the output state [3], [43], [48].

The MP-P protocol is an improvement of the MP-C protocol that exploits the existence of multiple trees to increase the multipartite DR. Thus, instead of terminating after generating a single GHZ state, the GHZ generation operations (lines 6–12) are repeated until a connecting tree can no longer be found. The protocol's name derives from the tree-packing problem, for finding the maximum number of Steiner trees in a graph.

C. PROTOCOL COMPARISON

A comparison of the main features of the proposed MP protocols and the SP protocol is shown in Table I. The number of nodes and edges in G is given by $|V|$ and $|E|$ respectively. Similarly, $|R|$ gives the number of edges in the routing solution R. In terms of scalability, the MP-G+ and SP protocols described require a center node to share a Bell pair with each user. Hence, the size of the GHZ state that can be distributed is limited by the number of quantum memories at the center

Algorithm 4: MP-P Protocol.

1: **function** MP-P(G, S)
2:   HasGHZ = **False**
3:   **while** *not* HasGHZ **do**
4:     SimulateEntanglementLinks(G)
5:     G' = updateLinkSubgraph(G)
6:     **while** hasConnectingTree(G', S) **do**
7:       R = minimumSteinerTree(G', S)
8:       EntanglementSwapping(G, R, S)
9:       EntanglementFusion(G, R, S)
10:      G' = updateLinkSubgraph(G)
11:      HasGHZ = **True**
12:    **end while**
13: **end while**
14: **end function**

TABLE I. Comparative Summary of Multipartite Routing Protocols

Protocol	Free scaling with users	Routing computational complexity (per timeslot)	Classical communication complexity
SP	No	$O(\|R\|)$	$O(\|R\|)$
MP-G+	No	$O(\|V\|^2\|E\|)$	$O(\|E\|)$
MP-C	Yes	$O(\|E\| + \|V\|log\|V\|)$	$O(\|E\|)$
MP-P	Yes	$O((\|E\| + \|V\|log\|V\|)\|V\|)$	$O(\|E\|)$

node (equal to the nodal degree of the center node). Therefore, these protocols do not freely scale with the number of users.

In terms of computational complexity, we consider the classical computation that must be performed per timeslot. As the SP protocol uses a precomputed path, the only per-timeslot operation required is verifying that all edges in R hold an entanglement link. In contrast, the MP protocols attempt routing operations every timeslot. The computational complexity is, therefore, dominated by the performance of these suboperations such as the Edmonds–Karp algorithm to calculate the multiple paths for the MP-G+ protocol ($O(\|V\|^2\|E\|)$) [46], [49] or Mehlhorn's approximate Steiner tree algorithm ($O(\|E\| + \|V\|log\|V\|)$) [50]. Finally, in terms of classical communication complexity (number of messages exchanged), the MP protocols require additional classical communication compared to SP protocols, as the state of G' must be obtained.

VI. PERFORMANCE EVALUATION: PROTOCOLS

The protocols were evaluated using a Monte Carlo simulation run on the quantum network model described in Section III. We compare the protocols in terms of the DR.

Throughout Section VI, we evaluated the protocols on a baseline scenario, varying one parameter at a time (i.e., p_e, the distance between users, numbers of users, and decoherence time). This baseline scenario was defined as a square grid topology of size $M \times M$ with $M = 6$ and $|S| = 4$ randomly located users in set $S \in V$. The entanglement link generation probability was uniform for all edges (i.e., $p_e = p$)
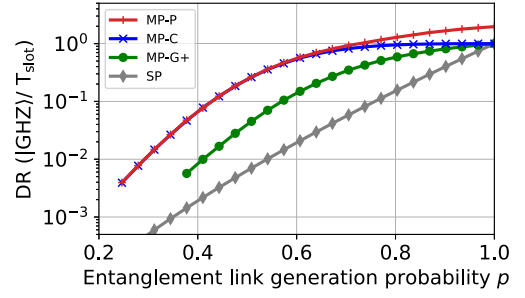

FIGURE 5. DR of $|GHZ_4\rangle$ states against entanglement link generation probability p in a 6 × 6 grid with $|S| = 4$ randomly located users ($M = 6$, $|S| = 4$, $p \in [0, 1]$, $Q_c = 1$).

and fixed at $p = 0.75$. The quantum memory decoherence was assumed to be sufficient to only store entanglement for a single timeslot (i.e., $Q_c = 1$). When plotting the data, unless otherwise stated, each data point in Figs. 5–14 represents the DR achieved by the protocols, averaged over 500 random user locations in the network. Each protocol was executed until a GHZ state was generated, or terminated after $t = 5000$ timeslots. If more than 5% of the protocol runs terminated without generating a GHZ state, the datapoint was not plotted.

A. EFFECT OF ENTANGLEMENT LINK GENERATION ON MULTIPARTITE STATE DR

Fig. 5 shows the DR of the proposed multipartite protocols as a function of p, with the performance of the SP protocol also shown for comparison. It can be observed that all three of the proposed multipartite protocols achieved a higher DR than the SP protocol. The simulation results show the MP-P and MP-C protocols achieved a DR approximately 38 times higher than the SP protocol at $p = 0.48$. The more flexible MP routing means GHZ states can be generated for more of the possible instances of G', e.g., different distributions of successful entanglement links in G'. We observe that the MP-P and MP-C protocols also outperform the MP-G+ protocol. This can be justified by considering the routing requirements of the protocols. The MP-P and MP-C protocols can use any Steiner tree of edges in G' for routing, whereas the MP-G+ protocol requires a separate edge-disjoint path between each user and the center node. As a result, the MP-P and MP-C protocols can generate GHZ state for more possible instances of G'. Additionally, all routing solutions that can be used by the MP-G+ protocol can also be used by the MP-P and MP-C protocols. Hence, these protocols will always achieve a DR greater than or equal to the MP-G+ protocol.

Finally, we observed that the MP-P protocol outperforms the MP-C protocol for $p \gtrsim 0.7$, where the MP-P protocol achieved a DR > 1. This occurs when on average multiple GHZ states are distributed per timeslot. This condition is met when there are multiple edge-disjoint Steiner trees connecting users in G'. As multiple trees are unlikely to exist below the percolation threshold, the MP-P performs comparably to the MP-C protocol for $p < 0.5$. As the average DR of
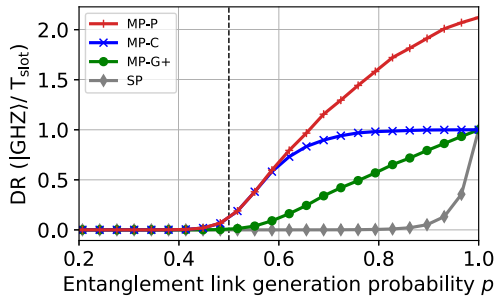
FIGURE 6. DR of $|GHZ_4\rangle$ states against entanglement link generation probability p in an 18 × 18 grid with $|S| = 4$ randomly located users ($M = 18$, $|S| = 4$, $p \in [0, 1]$, $Q_c = 1$).

FIGURE 7. DR of $|GHZ_4\rangle$ states between the four corner nodes against network grid size M (lower x-axis) and number of edges in the Steiner tree connecting the users (upper x-axis) ($M \in [3, 19]$, $|S| = 4$, $p = 0.75$, $Q_c = 1$).

the SP protocol has an analytical solution for $Q_c = 1$, the Monte Carlo simulation was not required to calculate the DR. Instead, the DR was found using (2) for a given routing solution R.

To better visualize the phase transition observed on systems exhibiting percolation, Fig. 6 replicates the results of Fig. 5 but in a larger 18 × 18 grid topology. Furthermore, the DR is shown on a linear scale, to better show the phase transition of DR against p. However, this approach does not allow for the visualization of DR for values spanning different orders of magnitude. Fig. 6 shows that the DR of the MP-P and MP-C protocols increase rapidly once percolation is observed ($p > 0.5$). For these protocols, the condition for successful routing is equivalent to all users being in the same connected component, which occurs with a high probability once a GCC exists. Because of the extra requirement of edge-disjoint paths, the phase transition is not as clear for the MP-G+ protocol.

B. DISTANCE-INDEPENDENT MULTIPARTITE STATE DR

A key benefit of MP routing shown in the literature is the ability to distribute entangled states, at a rate independent of the distance between the two users [26], [28]. We show that the developed MP protocols also achieve this result for multipartite states shared between multiple users. To demonstrate this, we simulate the protocols of grid networks of increasing size ($M \times M$ nodes), where the four corner nodes were selected as the users. The selection of corner nodes represents a worst case scenario for the MP protocols.

Fig. 7 shows the DR achieved, plotted against the width M of the grid topologies (lower x-axis). We define the number of edges in this Steiner tree in G as the distance between multiple users. For Fig. 7, this Steiner tree consists of $3 \times (M - 1)$ edges (value shown on the upper x-axis) and is a lower bound to the number of edges of a routing solution in G'. It can be seen that the MP protocols maintain a DR, which is constant with distance. In contrast, the DR achieved by the SP protocol decreases exponentially with distance. Consistent with Fig. 5, the MP-P and MP-C protocols achieved higher DRs than the MP-G+ protocol.

As the entanglement link generation probability is above the percolation threshold $p_c = 0.5$ of the given topology, the
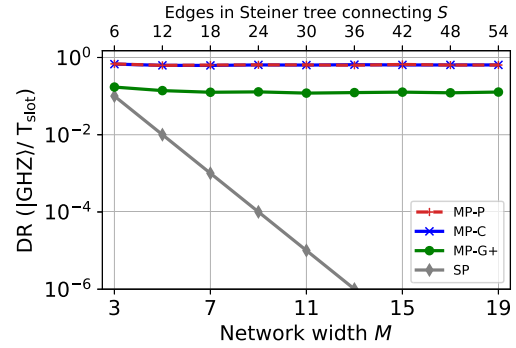
likelihood of all users being in the same connected component is the same regardless of the distance between the users. This is a sufficient condition for a routing solution to exist for the MP-P and MP-C protocols, and hence, the DR is independent of the distance between the users. These results show that the developed protocols can achieve distance-independent DR, even for multiple users sharing multipartite states. We use the metric *speedup* to quantify the relative performance of an MP protocol, compared to the benchmark SP protocol. The speedup is defined by the ratio of the DR achieved by a protocol, in comparison to the benchmark SP protocol under identical network conditions

$$\text{speedup} = \frac{DR_{\text{protocol}}}{DR_{\text{SP}}}. \qquad (3)$$

The speedup observed by the MP protocols was found to be of order $O((1/p)^{|S|})$ ($p_c < p \leq 1$, $|S| \geq 2$), showing an exponential speedup in the rate of multipartite state distribution for the MP protocols developed. The MP protocols achieve a DR, which scales with $O(1)$ for the distance between users, whereas for the SP protocols, DR $\sim O(p^{|R|})$ for a routing solution of size $|R|$. As $|R|$ will depend on the specific topology and location of users, we use $|R| \geq |S|$ to show the speedup is still exponential for the worst case when $|R| = |S|$. These results are valid when entanglement links are generated with p above the percolation threshold ($p_c = 0.5$ for grid lattices). For $p < p_c$, the DR achieved by the MP protocols decreases with the distance between users. However, the DR-distance scaling still significantly outperforms that of the SP protocol.

These distance-independent results were obtained assuming that entanglement links generated with ideal fidelities and subsequent LOCC operations are also error-free. In NISQ-era networks, these assumptions are not generally valid. For the proposed protocols, the fidelity of the distributed GHZ state will depend on the fidelities of the entanglement links used to generate the state [43] as well as the local operations performed [15]. This means that a true distance-independent distribution of GHZ states will not generally be feasible for NISQ-era networks, where local operations add error. However, we expect the MP protocols to scale with distance
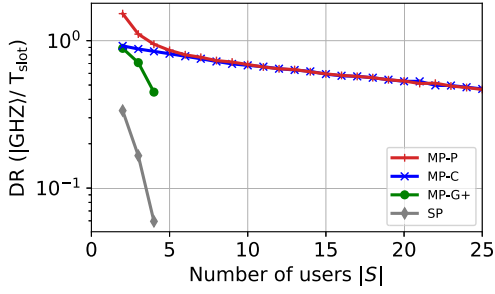
FIGURE 8. DR of $|GHZ_N\rangle$ states against increasing number of randomly located users, with $N = |S|$ ($M = 6$, $p = 0.75$, $|S| \in [3, 25]$, $Q_c = 1$).

FIGURE 9. DR of $|GHZ_4\rangle$ states by the MP-P protocol against entanglement link generation probability p for four randomly located users with selected values of Q_c. As a reference, the line DR = p is also plotted ($M = 6$, $|S| = 4$, $p \in [0, 1]$, $Q_c \in \{1, 2, 5, 10, \infty\}$).

significantly better than SP protocols operating in the same scenarios. This is because the MP protocols have a much higher probability of successful routing, independent of the effect of noisy local operations.

C. MULTIPARTITE STATE DR WITH VARIED USERS
The protocols were tested to assess the effect of the number of users on the DR. The number of users was varied between 3 and 25 in a 6×6 grid network. The users in S were randomly selected from the set of nodes V. As in Section VI-A, each datapoint represents the average of 500 different sets of users, which all contain the same number of users. Fig. 8 shows the DR achieved by the protocols in this scenario. Similar results were obtained in grid topologies of other sizes. Whereas the standard SP protocol exhibits an exponential decrease in DR with the number of users, the MP-P and MP-C protocols scaled significantly better. Furthermore, the size of the GHZ state generated by the MP-G+ and SP protocols was limited by the number of quantum memories available at the center node, as we assume one quantum memory per physical edge. In grid networks, these protocols can therefore service up to $|S| = 4$ users, with $|S| = 5$ only feasible if the center node is also a user.

As the MP-P and MP-C protocols do not require a central node, they can freely scale with the number of users. Furthermore, in contrast to SP routing, they exhibit a much smaller penalty to the DR for each additional user. For the MP-C protocol, a $|GHZ_{25}\rangle$ state was generated with a DR ≈ 0.5 This result is only valid above the critical probability $p > p_c$ for percolation, with distributing entanglement between large numbers of users being more challenging otherwise. A further result was that the benefit of MP-P was found to be more significant for fewer users, with a minimal benefit for using the MP-P protocol over MP-C beyond five users in the grid topology due to the absence of multiple disjoint Steiner trees in G'.

D. QUANTUM MEMORY DECOHERENCE EFFECT ON DR
We have demonstrated that our developed MP protocols can achieve an exponential speedup, compared to the SP protocol, for sharing multipartite states between multiple users. However, for maximum benefit, entanglement links must be generated with a probability above the critical probability of
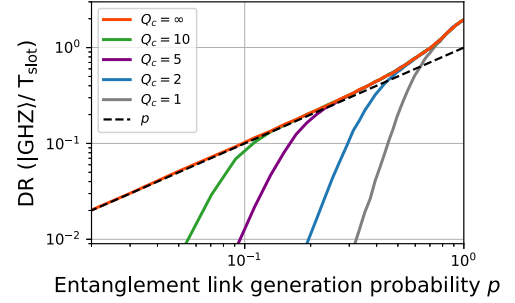
percolation for the given topology, which is currently infeasible for any realistic quantum network [51]. In this section, we further demonstrate how the benefits of MP routing can be observed, below the percolation threshold. This is achievable when the nodes are equipped with quantum memories able to store qubits for multiple timeslots.

Previous results consider only entanglement link generation for single independent timeslots ($Q_c = 1$), which is a common assumption in the literature [26]. However, this limits the possible functionality of the protocols. Patil et al. [42] consider a network model in which entanglement links are attempted for multiple timeslots, but also requires nodes be equipped with an additional quantum memory per edge per timeslot. Instead, we consider a single quantum memory per edge that can store an entanglement link over multiple timeslots.

To study the impact of quantum memory decoherence on the DR, we simulated the MP-P protocol for networks with varied quantum memory decoherence times. For each decoherence time Q_c analyzed, the value of Q_c was equal for all quantum memories in the network. Results in Fig. 9 show that networks with better quantum memories (i.e., higher Q_c) achieve a higher DR. However, we observe that increasing Q_c does not improve the DR when the protocol is already generating GHZ states at a DR greater than p (dashed black line). As this condition requires the GHZ state to be generated in fewer than Q_c timeslots, the protocols terminate before higher Q_c can influence the state of G'. Fig. 9 also shows the protocols achieve a DR, which improves rapidly with increasing p, until approaching $DR \approx p$ where DR growth decreases. The transition point between these two regimes occurs at approximately $p = 1/(Q_c + 1)$.

This transition can be explained by considering the probability of an entanglement link being present in a specific instance of G', $P(\omega(e) = 1)$. When $Q_c = 1$, this probability is equal to the entanglement link generation probability p_e. However, when entanglement links can be stored for multiple timeslots ($Q_c > 1$), the value of $P(\omega(e) = 1)$ also depends on the value of Q_c. We derive $P(\omega(e) = 1)$ as

$$P(\omega(e) = 1) = \frac{|\{\Omega_T | \omega(e) = 1\}|}{|\{\Omega_T | \omega(e) = 1\}| + |\{\Omega_T | \omega(e) = 0\}|} \quad (4)$$
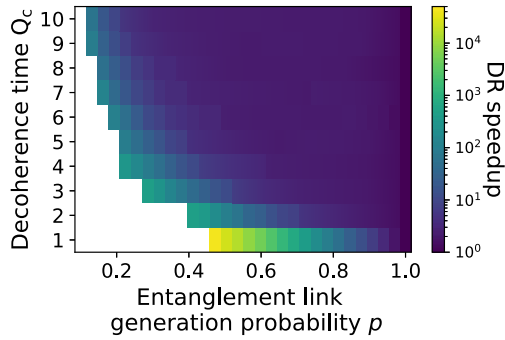
FIGURE 10. DR speedup of the MP-P protocol over the SP protocol when distributing $|GHZ_4\rangle$ states between the four corner nodes of a 6 × 6 grid topology, for a parameter sweep of p and Q_c ($M = 6$, $|S| = 4$, $p \in [0,1]$, $Q_c \in \{1, 2, \ldots, 10\}$).

TABLE II. Optical Networks Topologies With Network Edge Lengths Scaled Down by a Factor of 100 and the 6 × 6 Grid Topology [53]

Network Name	Number of nodes	Number of edges	Average edge length (km)	Average nodal degree
ARPA	20	31	6.09	3.1
EON	20	39	7.24	3.9
Eurocore	11	25	4.26	4.55
NSFnet	14	21	5.09	3.0
UKnet	21	39	1.38	3.71
USnet	46	76	4.34	3.3
Grid-6 (Section VI-A)	36	60	1.0	3.33

where $|\{\Omega_T | \omega(e) = x\}|$ is the number of timeslots for which $\omega(e) = x$, with $x \in \{0, 1\}$. For n attempts at entanglement link generation, we expect np_e to succeed and $n(1 - p_e)$ to fail. Each successfully generated entanglement link can remain present over the edge e for Q_c timeslots. Thus, $|\{\Omega_T | \omega(e) = 1\}|$ is equal to $np_e \times Q_c$. As each failed attempt lasts a single timeslot, then $|\{\Omega_T | \omega(e) = 0\}|$ equals $n(1 - p_e)$. Therefore, for a sufficiently large number of attempts, $P(\omega(e) = 1)$ is given in

$$P(\omega(e) = 1) = \frac{p_e Q_c}{p_e Q_c + (1 - p_e)}. \tag{5}$$

In topologies with homogeneous $P(\omega(e) = 1)$, percolation can be achieved when $P(\omega(e) = 1) > p_c$ [52]. Thus, by making the right side of (5) equal to 0.5, we get $p = 1/(Q_c + 1)$, which explains the observed transition. In Fig. 9, we see all protocols achieve similar DRs for values of p and Q_c, such that $P(\omega(e) = 1) > p_c$. Above this critical probability, we expect a single GCC in G', and therefore, a high DR of GHZ states is possible. There is a reduced growth in the DR when a GCC exists as there is a high probability all users are already connected. The MP protocols can achieve higher DRs over networks where entanglement links can be stored for multiple timeslots, even when the generation probability of the entanglement links is below p_c. This shows how improved quantum memories can increase the DRs of the developed MP routing protocols.

To quantify the relative performance of the MP-P and SP protocol, a wider parameter sweep of p and Q_c was performed in a 6 × 6 grid topology with four users located in the corner nodes of the network. Fig. 10 shows the speedup of the MP-P protocol compared to the SP protocol. The white area shows data points where more than 5% of simulation runs failed to generate a GHZ state.

A speedup in DR was observed for all values of $Q_c \geq 1$ and $0 < p \leq 1$. The largest DR speedup was observed for $p = 0.47$, $Q_c = 1$, with a 4×10^4 improvement. Similar speedups, of different magnitudes, were observed for different-sized grid topologies and for randomly located users. The high DR speedup for these network conditions

suggests that the proposed protocols will be useful for NISQ-era networks, where networks consist of devices with short decoherence times and low DRs. Fig. 10 also shows that with larger Q_c, the DR speedup becomes significant at lower values of p. This shift occurs due to the effect of Q_c on $P(\omega(e) = 1)$. While both the MP-P and SP protocols achieve a higher DR with higher Q_c, the magnitude of the speedup is reduced mainly due to the relative improvement of the SP protocol. As was shown in Fig. 9, the MP-P protocol can achieve higher DR at low p, by increasing Q_c. These results demonstrate that the proposed MP protocols improve the multipartite state DR.

VII. PERFORMANCE EVALUATION: MESH TOPOLOGIES
The protocols developed can be applied to any topology, but the achievable DRs might differ depending on the topology. To investigate this we simulated the best performing protocol, MP-P, on topologies taken from real-world optical networks, which are described in Table II [53]. The edge lengths of the topologies used were scaled down by a factor of 100, to more closely match the size of current experimental entanglement distribution setups [51]. The entanglement link generation probability p_e was calculated for each edge using (1). To parameterize p_e, we vary p_{op}, with p_{loss} a fixed function of edge length. Furthermore, for the mesh topologies, we only consider networks with $Q_c = 1$. The legend identifying the topologies in Fig. 11 also applies to later figures in this section. Performance was evaluated with varied entanglement link generation probabilities and numbers of users.

A. DR SPEEDUP IN MESH TOPOLOGIES
We plot the DR against average edge probabilities $\bar{p}_e$, to allow for easier comparison among topologies with a variety of edge lengths and, therefore, values of p_e. We used randomly located users with $|S| = 5$ and $Q_c = 1$. Fig. 11 shows that the DR followed a similar trend as seen in the grid topologies with uniform p. However, the absolute DR achieved by the protocols varied among topologies, especially at low $\bar{p}_e$. Furthermore, the topologies in which the highest DR was achieved (Eurocore, EON, and UKNet) had a wide range of average edge lengths among them. This suggested that multiple factors, such as nodal degree, edge length, and network size, all affect the achievable DR.
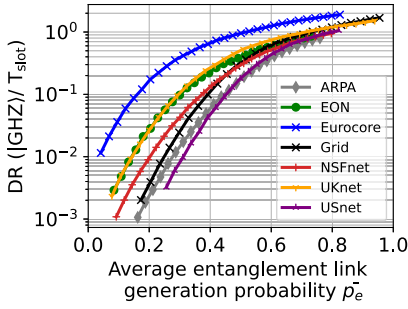
FIGURE 11. DR of $|\text{GHZ}_5\rangle$ states by the MP-P protocol against average entanglement link generation probability $\bar{p}_e$ for five users randomly located in each topology. $\bar{p}_e$ was varied by sweeping the parameter p_{op}. The legend used also applies to later figures in Section VII ($|S| = 5$, $p_{op} \in [0, 1]$, $Q_c = 1$).

FIGURE 12. DR speedup of the MP-P protocol over the SP protocol against $\bar{p}_e$ when distributing $|\text{GHZ}_5\rangle$ states between five randomly located users ($|S| = 5$, $p_{op} \in [0, 1]$, $Q_c = 1$).

The speedup of the MP-P protocol over the SP protocol on the varied topologies is shown in Fig. 12. For the mesh topologies we compare the DR against the tree variant of the SP routing [25]. In this approach, routing is performed along the Steiner tree in G. We use this more general protocol in the mesh topologies as it is more robust to networks with varied edge degrees. Hence, the location of a valid center node will not affect the DR achieved by the SP protocol.

For all topologies, a significant speedup occurred for all values of $\bar{p}_e$, with a maximum at an intermediate value of $\bar{p}_e$. Depending on topology, the maximum speedup was observed between $0.28 < \bar{p}_e < 0.53$. For the Grid-6 network, the maximum speedup occurred at $\bar{p}_e = 0.52$, close to the percolation threshold for this topology. The speedup achieved by the MP-P protocol was found to be reduced for both high and low $\bar{p}_e$. For high $\bar{p}_e$, the SP protocol was sufficient to obtain a high DR; hence, the relative speedup achievable for the MP-P protocol decreased. Similarly, for very low $\bar{p}_e$, we suggest that routing will predominately succeed along the minimum distance tree in G', as longer trees will exist with a significantly lower likelihood. This also reduces the benefit of the proposed MP protocols. However, the results suggest a significant DR improvement will still be achieved for low $\bar{p}_e$. At intermediate values of $\bar{p}_e$, there was sufficient redundancy in the edge distribution of the subgraph G', such that routing succeeded with a high rate for MP protocol. In contrast, the SP protocol has a much reduced DR as a single entanglement link failure along the route prevents a GHZ state from being generated. The magnitude of the speedup was found to be lower compared to that seen in Fig. 10. This is primarily due to the choice of users rather than a feature of the topologies. By using randomly located users, instead of users in distantly located nodes, the average distance between users was lower, and hence, the magnitude of the speedup was reduced.

B. SCALING WITH USERS IN MESH TOPOLOGIES

The MP-P protocol was further studied on the mesh topologies to assess the impact of the number of users on the DR. Performance was evaluated for two values of operational probability p_{op} as shown in Fig. 13(a) $p_{op} = 0.75$ and (b)
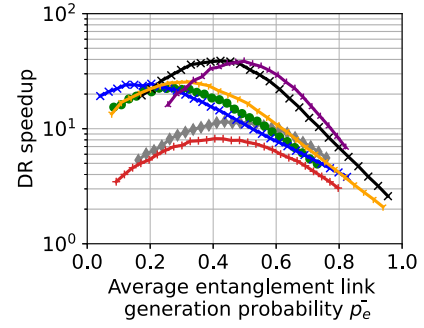
$p_{op} = 0.4$. The results show that the DR decreases for additional users, as seen in Fig. 8 for the grid topology. Additionally, there is a significant variation in the DR scaling behavior between topologies. Certain topologies such as the Eurocore, UKnet, and Grid-6 networks achieve high DRs even for a large number of users. This was thought to be primarily due to their higher nodal degree. For the MP protocols, being able to utilize many possible paths means that a high nodal degree improves DR.

However, the ordering of DR achieved by the protocols in different topologies was not consistent for all values of p_{op}. For example, Fig. 13(a) shows the grid topology (black line) performed better at $p_{op} = 0.75$ relative to the other topologies than at $p_{op} = 0.4$ [see Fig. 13(b)]. This behavior might be explained by considering the size of the largest connected component of G', which for these networks will be a function of p_{op} and topology [32], [54]. Fig. 13(c) shows the proportion of network nodes belonging to the largest connected component with varied p_{op}. These mesh topologies do not have defined percolation thresholds, with the proportion of nodes in the largest connected component following a continuous distribution with p_{op}. However, the size of the largest connected component at $p_{op} = 0.4$ and $p_{op} = 0.75$ correlates with variation in relative performance observed between the topologies. In Section VIII, we relate the relationship between the DR and the connected component size analytically.

VIII. ANALYTICAL DR

The Monte Carlo simulation model allows for varied protocols and network models to be simulated. However, this approach is computationally intensive when simulating low DR values. Therefore, analytical expressions for the DR were reviewed in Section VIII-A and proposed in Section VIII-B. The developed analytical approach allowed fast comparison of network parameters, such as topology, on the protocols.

A. ANALYTICAL APPROXIMATIONS

We define the upper bound of the DR as the maximum number of GHZ states that can be distributed per timeslot. From the graph definition of the network, this upper bound
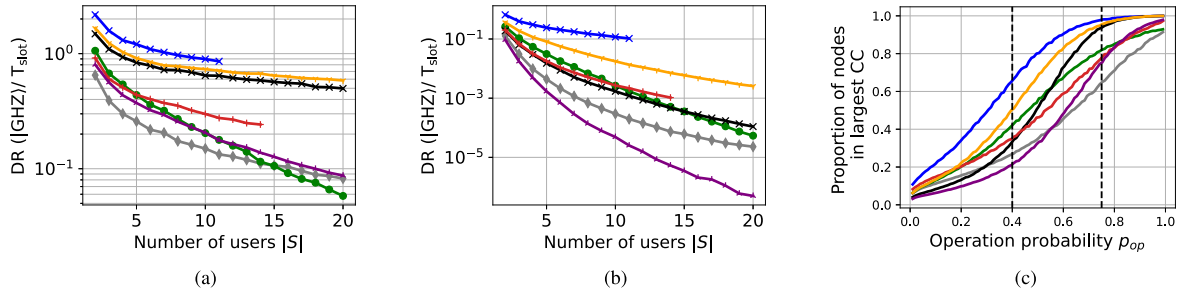
FIGURE 13. (a) DR of $|GHZ_N\rangle$ states, N = |S|, for the MP-P protocol with number of users |S| and p_{op} = 0.75. (b) DR of $|GHZ_N\rangle$ states, N = |S|, for the MP-P protocol with number of users |S| and p_{op} = 0.4. (c) Proportion of nodes that are part of the GCC in G' (Q_c = 1).

equals the number of edge-disjoint Steiner trees connecting the users in G. Similarly, for a given timeslot, the number of GHZ states that can be distributed is the number of such trees in G'. Finding the number of edge-disjoint trees in a graph is the Steiner tree packing problem [55]. However, due to the hardness of solving this problem directly, an equivalent upper bound was instead considered. This equivalent is the minimum cut of edges in G to separate a user from the set of other users. For the grid topology, this min-cut is the nodal degree of a user, giving an upper bound of DR $\leq 4P(\omega(e) = 1)$. The protocols developed were not found to approach this upper bound for any values of p. This suggests that routing multiple GHZ states in G' is challenging, even for networks where entanglement links are present with a probability above the critical threshold for percolation.

Given the performance of the previous bound, a separate approach considers estimating DR by calculating the probability of all users S being in the same connected C component, $P(S \in C)$. For graphs with probabilistic edges, finding this probability is known as the k-terminal reliability problem [56], [57]. In general topologies, this problem is NP-hard, but if percolation can be assumed then simplified models can be utilized [58]. For infinite lattices in percolation, the term $\theta(p)$ gives the probability of a node being part of the GCC [31]. The probability of all users being in this GCC is given by $P(S \in GCC) = \theta(p)^{|S|}$. However, in the finite topologies considered, this expression is not accurate for values of $p < p_c$. Therefore, it cannot be used for low computational complexity estimation of DR for the scenarios considered in this article.

B. IMPROVED APPROXIMATION

For small graphs, the term $\theta(p)^{|S|}$ can not be used to find $P(S \in GCC)$. We can instead substitute $\theta(p)$ with $|C|/|V|$, where C is the largest connected component in G'. However, this approach also assumes that each event $(s \in C), \forall s \in S$ is independent, which is not the case when $|S| \approx |C|$, such as below percolation.

Thus, to get a better approximation for the probability $P(S \in C)$, we modeled this as a *Hypergeometric discrete probability distribution* [59]. The Hypergeometric distribution describes the probability of k successes in n draws *without replacement* from an X-sized population. Making $k =$

$|S|, n = |C|$, and $X = |V|$, this is equivalent to the probability of obtaining the nodes of S, after randomly selecting $|C|$ nodes from V without replacement. Therefore, the probability of all $|S|$ nodes of S being in a connected component C is given by

$$P(S \in C) \approx M(V, S, C) = \frac{\binom{|V|-|S|}{|C|-|S|}}{\binom{|V|}{|C|}}. \qquad (6)$$

The term $\binom{|V|}{|C|}$ gives the number of combinations of unique connected components of size $|C|$ that can be found from the nodes V. Similarly, $\binom{|V|-|S|}{|C|-|S|}$ is the number of ways a set S can be arranged in C. Combined, these expressions give the proportion of events for which a random connected component of size $|C|$ includes all users S.

For the MP-C and MP-P protocols, a valid routing solution only requires that all users are in the same connected component of G'. Below the percolation threshold, no GCC exists, and therefore, the size of the largest connected component C will be some probability distribution that is a function of p and the network topology. The probability of the largest connected component in G' having i nodes ($|C_i|$) is given by $\alpha_i = P(|C_i| = i)$ where $\sum_{i=1}^{|V|} \alpha_i = 1$. We found the values of α_i by numerically simulating G'. The DR can then be estimated using a weighted sum of (6) with α_i as the weights

$$DR \approx \sum_{i=1}^{|V|} \alpha_i \times M(V, S, C_i). \qquad (7)$$

Fig. 14 shows the closeness of fit between the DR calculated by Monte Carlo simulation of the MP-C protocol and from (7). This means this analytical expression can be used to calculate the DR where it is not computationally efficient to use a Monte Carlo simulation. More exact methods may be used that work for networks that operate strictly above the percolation threshold [54], [58], [60].

IX. CONCLUSION

We propose three protocols, MP-G+, MP-C, and MP-P, for the distribution of shared multipartite states across a quantum network. The protocols were designed to use MP routing, in order to improve the multipartite DR. These protocols were simulated on quantum networks and modeled to consider
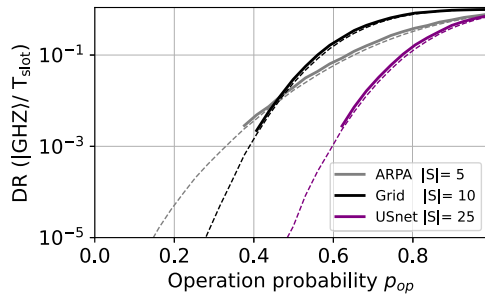
FIGURE 14. DR of $|GHZ_N\rangle$ states, N = |S|, of the MP-C protocol versus operational probability p_{op}. The DR of the MP-C protocol was calculated using both the Monte Carlo simulation (solid line) and using (7) (dashed). The values were found for a subset of topologies and number |S| of randomly located users ($Q_c = 1$).

probabilistic Bell pair distribution and qubit decoherence, such as would be observed in a network of NISQ devices.

The effect of network topology on the proposed protocols was assessed by simulating the protocols on topologies taken from real optical networks. The results show that the achieved DR varied between topologies, with features such as network size and average nodal degree found to have an effect. An analytical approximation using the probability distribution of successfully distributed Bell pairs was found to quantify these effects.

Results show that the proposed protocols all achieved an exponential speedup in the rate of multipartite state distribution. This speedup was observed with the distance between users when compared to protocols using SP routing. The observed speedup increased for many users, and when Bell pairs were distributed with a probability close to the percolation threshold for the given network topology. Of the protocols developed, the MP-P protocol achieved the highest rate of multipartite state distribution and when simulated achieved a speedup of up to four orders of magnitude. The use of quantum memories with improved decoherence times was considered. While improved quantum memories improved the multipartite DR for all protocols considered, the speedup of the MP protocols was most significant for short decoherence times. As the MP protocols provide speedup for intermediate values of entanglement generation and short decoherence times, this research will have possible applications for NISQ quantum networks.

REFERENCES

[1] S. Wehner, D. Elkouss, and R. Hanson, "Quantum internet: A vision for the road ahead," *Science*, vol. 362, no. 6412, Art. no. eaam9288, 2018, doi: 10.1126/science.aam9288.

[2] D. Cuomo, M. Caleffi, and A. S. Cacciapuoti, "Towards a distributed quantum computing ecosystem," *IET Quantum Commun.*, vol. 1, no. 1, pp. 3–8, 2020, doi: 10.48550/arXiv.2002.11808.

[3] C. H. Bennett, G. Brassard, S. Popescu, B. Schumacher, J. A. Smolin, and W. K. Wootters, "Purification of noisy entanglement and faithful teleportation via noisy channels," *Phys. Rev. Lett.*, vol. 76, no. 1, pp. 722–725, Jan. 1996, doi: 10.1103/PhysRevLett.76.722.

[4] C. Ren and H. F. Hofmann, "Clock synchronization using maximal multipartite entanglement," *Phys. Rev. A*, vol. 86, no. 1, 2012, Art. no. 014301, doi: 10.48550/arXiv.1203.4300.

[5] Z. Zhang and Q. Zhuang, "Distributed quantum sensing," *Quantum Sci. Technol.*, vol. 6, no. 4, 2021, Art. no. 043001, doi: 10.48550/arXiv.2010.14744.

[6] R. Cleve, D. Gottesman, and H.-K. Lo, "How to share a quantum secret," *Phys. Rev. Lett.*, vol. 83, pp. 648–651, Jul. 1999, doi: 10.1103/PhysRevLett.83.648.

[7] B. Bell et al., "Experimental demonstration of graph-state quantum secret sharing," *Nature Commun.*, vol. 5, no. 1, pp. 1–12, 2014, doi: 10.48550/arXiv.1411.5827.

[8] G.-B. Xu, Q.-Y. Wen, F. Gao, and S.-J. Qin, "Novel multiparty quantum key agreement protocol with GHZ states," *Quantum Inf. Process.*, vol. 13, no. 12, pp. 2587–2594, 2014, 10.1007/s11128-014-0816-9.

[9] A. S. Cacciapuoti, M. Caleffi, F. Tafuri, F. S. Cataliotti, S. Gherardini, and G. Bianchi, "Quantum internet: Networking challenges in distributed quantum computing," *IEEE Netw.*, vol. 34, no. 1, pp. 137–143, Jan./Feb. 2020, doi: 10.1109/MNET.001.1900092.

[10] J. I. Cirac, A. K. Ekert, S. F. Huelga, and C. Macchiavello, "Distributed quantum computation over noisy channels," *Phys. Rev. A*, vol. 59, pp. 4249–4254, Jun. 1999, doi: 10.1103/PhysRevA.59.4249.

[11] S. DiAdamo, M. Ghibaudi, and J. Cruise, "Distributed Quantum Computing and Network Control for Accelerated VQE," *IEEE Trans. Quantum Eng.*, Institute of Electrical and Electronics Engineers (IEEE), vol. 2, 2021, pp. 1–21, doi: 10.1109/tqe.2021.3057908.

[12] P. Zhou and L. Lv, "Hyper-parallel nonlocal CNOT operation with hyperentanglement assisted by cross-Kerr nonlinearity," *Sci. Rep.*, vol. 9, no. 1, Nov. 2019, Art. no. 15939, doi: 10.1038/s41598-019-52173-x.

[13] N. H. Nickerson, Y. Li, and S. C. Benjamin, "Topological quantum computing with a very noisy network and local error rates approaching one percent," *Nature Commun.*, vol. 4, no. 1, pp. 1–5, 2013, doi: 10.48550/arXiv.1211.2217.

[14] L. Bugalho, F. A. Monteiro, B. Coutinho, and Y. Omar, "Distributing multipartite entanglement over noisy quantum networks," *Quantum*, vol. 7, pp. 920–945, Feb. 2023, doi: 10.48550/arXiv.2103.14759.

[15] P. Nain, G. Vardoyan, S. Guha, and D. Towsley, "On the analysis of a multipartite entanglement distribution switch," *Proc. ACM Meas. Anal. Comput. Syst.*, vol. 4, no. 2, pp. 1–39, 2020, doi: 10.48550/arXiv.2212.01784.

[16] T. Coopmans et al., "NetSquid, a network simulator for quantum information using discrete events," *Commun. Phys.*, vol. 4, no. 1, Jul. 2021, Art. no. 164, doi: 10.1038/s42005-021-00647-8.

[17] H.-J. Briegel, W. Dür, J. I. Cirac, and P. Zoller, "Quantum repeaters: The role of imperfect local operations in quantum communication," *Phys. Rev. Lett.*, vol. 81, pp. 5932–5935, Dec. 1998, doi: 10.1103/PhysRevLett.81.5932.

[18] W. J. Munro, K. Azuma, K. Tamaki, and K. Nemoto, "Inside quantum repeaters," *IEEE J. Sel. Topics Quantum Electron.*, vol. 21, no. 3, pp. 78–90, May/Jun. 2015, doi: 10.1109/JSTQE.2015.2392076.

[19] E. D'Hondt and P. Panangaden, "The computational power of the W and GHZ states," *J. Quantum Inf. Computation*, vol. 6, no. 2, pp. 173–183, 2005, doi: 10.48550/arXiv.quant-ph/0412177.

[20] L. Xiao, G. Lu Long, F.-G. Deng, and J.-W. Pan, "Efficient multiparty quantum-secret-sharing schemes," *Phys. Rev. A*, vol. 69, May 2004, Art. no. 052307, doi: 10.1103/PhysRevA.69.052307.

[21] K. Azuma, S. Bäuml, T. Coopmans, D. Elkouss, and B. Li, "Tools for quantum network design," *AVS Quantum Sci.*, vol. 3, no. 1, 2021, Art. no. 014101, doi: 10.48550/arXiv.2012.06764.

[22] S. Bäuml, K. Azuma, G. Kato, and D. Elkouss, "Linear programs for entanglement and key distribution in the quantum internet," *Commun. Phys.*, vol. 3, no. 1, pp. 1–12, 2020, doi: 10.48550/arXiv.1809.03120.

[23] B. Li, T. Coopmans, and D. Elkouss, "Efficient optimization of cut-offs in quantum repeater chains," in *Proc. IEEE Int. Conf. Quantum Comput. Eng.*, 2020, pp. 158–168, doi: 10.48550/arXiv.2005.04946.

[24] G. Avis, F. Rozpędek, and S. Wehner, "Analysis of multipartite entanglement distribution using a central quantum-network node," *Phys. Rev. A*, vol. 107, no. 1, 2023, Art. no. 012609, doi: 10.1103/PhysRevA.107.012609.

[25] C. Meignant, D. Markham, and F. Grosshans, "Distributing graph states over arbitrary quantum networks," *Phys. Rev. A*, vol. 100, no. 5, 2019, Art. no. 052333, doi: 10.48550/arXiv.1811.05445.

[26] M. Pant et al., "Routing entanglement in the quantum internet," *npj Quantum Inf.*, vol. 5, no. 1, 2019, Art. no. 25, doi: 10.48550/arXiv.1708.07142.

[27] S. Pirandola, "End-to-end capacities of a quantum communication network," *Commun. Phys.*, vol. 2, no. 1, 2019, Art. no. 51, doi: 10.48550/arXiv.1905.12674.

[28] A. Acín, J. I. Cirac, and M. Lewenstein, "Entanglement percolation in quantum networks," *Nature Phys.*, vol. 3, no. 4, pp. 256–259, 2007, doi: 10.48550/arXiv.quant-ph/0612167.

[29] S. Pirandola, R. Laurenza, C. Ottaviani, and L. Banchi, "Fundamental limits of repeaterless quantum communications," *Nature Commun.*, vol. 8, no. 1, Apr. 2017, Art. no. 15043, doi: 10.1038/ncomms15043.

[30] M. Molloy and B. Reed, "The size of the giant component of a random graph with a given degree sequence," *Combinatorics, Probability, Comput.*, vol. 7, no. 3, pp. 295–305, 1998, doi: 10.1017/S0963548398003526.

[31] G. Grimmett, *Percolation, ser. Grundlehren der mathematischen Wissenschaften*. Berlin, Germany: Springer 2013, doi: 10.1007/978-3-662-03981-6. [Online]. Available: https://books.google.co.uk/books?id=Vnz1CAAAQBAJ

[32] D. Stauffer and A. Aharony, *Introduction to Percolation Theory*. New York, NY, USA: Taylor & Francis, 2018, doi: 10.1201/9781315274386.

[33] R. Laurenza, N. Walk, J. Eisert, and S. Pirandola, "Rate limits in quantum networks with lossy repeaters," *Phys. Rev. Res.*, vol. 4, no. 2, 2022, Art. no. 023158, doi: 10.48550/arXiv.2110.10168.

[34] A. Patil, J. I. Jacobson, E. Van Milligen, D. Towsley, and S. Guha, "Distance-independent entanglement generation in a quantum network using space-time multiplexed Greenberger–Horne–Zeilinger (GHZ) measurements," in *Proc. IEEE Int. Conf. Quantum Comput. Eng.*, 2021, pp. 334–345, doi: 10.1109/QCE52317.2021.00050.

[35] A. Patil, M. Pant, D. Englund, D. Towsley, and S. Guha, "Entanglement generation in a quantum network at distance-independent rate," *npj Quantum Inf.*, vol. 8, no. 1, May 2022, Art. no. 51, doi: 10.1038/s41534-022-00536-0.

[36] Y. Zhao and C. Qiao, "Redundant entanglement provisioning and selection for throughput maximization in quantum networks," in *Proc. IEEE INFOCOM Conf. Comput. Commun.*, 2021, pp. 1–10, doi: 10.1109/INFOCOM42981.2021.9488850.

[37] E. Sutcliffe, M. J. Hoban, and A. Beghelli, "Multi-user entanglement routing for quantum mesh networks," in *Opt. Fiber Commun. Conf. Exhibit.*, 2023, pp. 1–3, doi: 10.1364/OFC.2023.W4K.2.

[38] E. Sutcliffe, M. J. Hoban, and A. Beghelli, "Multipath routing for multipartite state distribution in quantum networks," in *Proc. Quantum 2.0 Conf. Exhibit.*, 2023, Art. no. QTu2A-23, doi: 10.1364/QUANTUM.2022.QTu2A.23.

[39] X. Han, W. Fu, C.-L. Zou, L. Jiang, and H. X. Tang, "Microwave-optical quantum frequency conversion," *Optica*, vol. 8, no. 8, pp. 1050–1064, 2021, doi: 10.1364/OPTICA.425414.

[40] G. Chiribella, G. M. D'Ariano, P. Perinotti, and B. Valiron, "Quantum computations without definite causal structure," *Phys. Rev. A*, vol. 88, Aug. 2013, Art. no. 022318, doi: 10.1103/PhysRevA.88.022318.

[41] Y. Lee, E. Bersin, A. Dahlberg, S. Wehner, and D. Englund, "A quantum router architecture for high-fidelity entanglement flows in quantum networks," *npj Quantum Inf.*, vol. 8, no. 1, 2022, Art. no. 75, doi: 10.48550/arXiv.2005.01852.

[42] P. Dhara, A. Patil, H. Krovi, and S. Guha, "Subexponential rate versus distance with time-multiplexed quantum repeaters," *Phys. Rev. A*, vol. 104, Nov. 2021, Art. no. 052612, doi: 10.1103/PhysRevA.104.052612.

[43] S. de Bone, R. Ouyang, K. Goodenough, and D. Elkouss, "Protocols for creating and distilling multipartite GHZ states with Bell pairs," *IEEE Trans. Quantum Eng.*, vol. 1, 2020, Art. no. 4102710, doi: 10.1109/TQE.2020.3044179.

[44] H. Bernien et al., "Heralded entanglement between solid-state qubits separated by three metres," *Nature*, vol. 497, no. 7447, pp. 86–90, 2013, doi: 10.48550/arXiv.1212.6136.

[45] N. Megiddo, "Optimal flows in networks with multiple sources and sinks," *Math. Program.*, vol. 7, no. 1, pp. 97–107, 1974, doi: 10.1007/BF01585506.

[46] J. Edmonds and R. M. Karp, "Theoretical improvements in algorithmic efficiency for network flow problems," *J. ACM*, vol. 19, no. 2, pp. 248–264, 1972, doi: 10.1145/321694.321699.

[47] F. Grasselli, H. Kampermann, and D. Bruß, "Finite-key effects in multipartite quantum key distribution protocols," *New J. Phys.*, vol. 20, no. 11, 2018, Art. no. 113014, doi: 10.48550/arXiv.1807.04472.

[48] S. Krastanov, A. S. de la Cerda, and P. Narang, "Heterogeneous multipartite entanglement purification for size-constrained quantum devices," *Phys. Rev. Res.*, vol. 3, no. 3, 2021, Art. no. 033164, doi: 10.48550/arXiv.2011.11640.

[49] Y. Dinitz, "Dinitz' algorithm: The original version and even's version," in *Theoretical Computer Science: Essays Memory Shimon Even*. Berlin, Germany: Springer, pp. 218–240, 2006, doi: 10.1007/11685654_10.

[50] K. Mehlhorn, "A faster approximation algorithm for the Steiner problem in graphs," *Inf. Process. Lett.*, vol. 27, no. 3, pp. 125–128, 1988, doi: 10.1016/0020-0190(88)90066-X.

[51] Y. Yu et al., "Entanglement of two quantum memories via fibres over dozens of kilometres," *Nature*, vol. 578, no. 7794, pp. 240–245, 2020, doi: 10.48550/arXiv.1903.11284.

[52] B. Bollobás and O. Riordan, "Basic concepts and results," *Percolation*. Cambridge, U.K.: Cambridge Univ. Press, 2006, pp. 1–35, doi: 10.1017/CBO9781139167383.

[53] S. Baroni, "Routing and wavelength allocation in WDM optical networks," Ph.D. dissertation, Dept. Electron. Elec. Eng., Univ. College London, London, U.K., 1998. [Online]. Available: https://discovery.ucl.ac.uk/id/eprint/10100693

[54] M. E. Newman, S. H. Strogatz, and D. J. Watts, "Random graphs with arbitrary degree distributions and their applications," *Phys. Rev. E*, vol. 64, no. 2, 2001, Art. no. 026118, doi: 10.48550/arXiv.cond-mat/0007235.

[55] K. Jain, M. Mahdian, and M. R. Salavatipour, "Packing Steiner trees," in *Proc. 14th Annu. ACM-SIAM Symp. Discrete Algorithms*, 2003, pp. 266–274. [Online]. Available: https://dl.acm.org/doi/10.5555/644108.644154

[56] S. Reed, M. Löfstrand, and J. Andrews, "An efficient algorithm for computing exact system and survival signatures of k-terminal network reliability," *Rel. Eng. Syst. Saf.*, vol. 185, pp. 429–439, 2019, doi: 10.1016/j.ress.2019.01.011.

[57] R. Zenklusen, "Combinatorial methods for analyzing network security and reliability," Ph.D. dissertation, Dept. Math., ETH Zurich, Zurich, Switzerland, 2008.

[58] M. Newman, *Networks*. London, U.K.: Oxford Univ. Press, 2018, doi: 10.1093/oso/9780198805090.001.0001.

[59] S. M. Ross, *Introduction to Probability Models*. New York, NY, USA: Academic, 2014, doi: 10.1016/C2012-0-03564-8.

[60] M. Kitsak et al., "Stability of a giant connected component in a complex network," *Phys. Rev. E*, vol. 97, no. 1, 2018, Art. no. 012309, doi: 10.1103/PhysRevE.97.012309.